

Dual-Flow Transformation Network for Deformable Image Registration with Region Consistency Constraint

Xinke Ma¹, Yibo Yang², Yong Xia^{1*}, Dacheng Tao²

School of Computer Science and Engineering, Northwestern Polytechnical University, China¹
 JD Explore Academy, JD.com Inc, Beijing, China²

{ yxia@nwpu.edu.cn, maxxk@foxmail.com }

Abstract

Deformable image registration is able to achieve fast and accurate alignment between a pair of images and thus plays an important role in many medical image studies. The current deep learning (DL)-based image registration approaches directly learn the spatial transformation from one image to another by leveraging a convolutional neural network, requiring ground truth or similarity metric. Nevertheless, these methods only use a global similarity energy function to evaluate the similarity of a pair of images, which ignores the similarity of regions of interest (ROIs) within images. Moreover, DL-based methods often estimate global spatial transformations of image directly, which never pays attention to region spatial transformations of ROIs within images. In this paper, we present a novel dual-flow transformation network with region consistency constraint which maximizes the similarity of ROIs within a pair of images and estimates both global and region spatial transformations simultaneously. Experiments on four public 3D MRI datasets show that the proposed method achieves the best registration performance in accuracy and generalization compared with other state-of-the-art methods.

1. Introduction

Deformable image registration is widely applied to many medical imaging studies such as detecting temporal anatomical changes of individuals [48], analyzing variability across populations [44], and multi-modality fusion [9]. Deformable image registration is to establish the non-linear correspondence between a pair of images and estimate the appropriate nonlinear transformation to align a pair of images [31]. Medical professionals analyze the regions of interest (ROIs) in a unified anatomical space, which plays an important role in many clinical applications [6, 12, 34, 40]. Traditional deformable image registration [3, 32, 37, 45] is

an iterative optimization process. Unfortunately, iterative methods are extremely slow, which cannot achieve realtime registration in clinical operations [29].

Recently, deep learning (DL)-based methods [5, 10, 19] have gained increasing popularity in the field of deformable image registration. DL-based methods [2, 16, 26, 28, 33] learn a universal representations of data samples using convolutional neural networks (CNN) to estimate corresponding deformation between the moving and fixed images. These methods achieve rapid deformable image registration, making possible the realtime registration in practical applications. However, these approaches [21, 31, 38, 39, 41] only learn global correspondence of a pair of images to obtain displacement flow fields (DFFs) and ignore the similarity of regions of interest (ROIs) within images. In addition, these methods only use a global similarity metric to evaluate the similarity of a pair of images, which cannot maximize the similarity of ROIs within a pair of images. Furthermore, label-constrained (LC) registration methods [13, 19, 20, 27] have been developed to enhance the correspondence of ROIs between a pair of images. LC registration approaches [5, 18, 30, 42] are capable of leveraging auxiliary information such as segmentation labels, and thus the appearance structure of ROIs can be perceived, which further enhances the similarity of ROIs within images. Nevertheless, the segmentation labels are lacking of texture information constraining the correspondence action to only focus on the alignment of the ROIs edges and ignore the texture of ROIs, which leads to the distortions on ROIs. Therefore, this deformation will distort the texture of the ROIs and make the deformed images less convincing.

Motivation: Inspired by LC-based registration approaches, we use segmentation CNN to perceive texture-preserved ROIs within images by leveraging segmentation labels and original images. Meanwhile, we present a novel dual-flow transformation network with a region consistency constraint to maximize the similarity of ROIs within images and improve registration accuracy. Specifically, a dual-flow transformation network is proposed to achieve coarse-to-

*corresponding author

fine registration, which includes two main steps: (i) Region-aware deformable transformation between a pair of images is performed to recognize ROIs within images, which achieves a region-aware alignment; (ii) Global deformable transformation is employed to further dig out potential ROIs within images to achieve a fine registration. The ROIs with texture information are used to learn DFFs obviating the interference of task-unconcerned regions. Furthermore, a region consistency constraint is developed to maximize the ROIs similarity of a pair of images. Specifically, we have made the following contributions:

- A dual-flow transformation network is developed to perceive ROIs within images to weaken the interference of task-unconcerned regions and achieve a region-aware registration between a pair of images. It is able to eliminate mis-alignment on ROIs and weaken distortion on ROIs.
- A region consistency constraint is proposed to guarantee the consistency between region-aware flow transformation and global flow transformation, which maximizes the ROIs similarity within a pair of images, thus improving registration accuracy.
- Extensive experiments on four public 3D MRI datasets were conducted, and our results show that the proposed method achieves substantially better registration performance in accuracy, stability and generalization than five state-of-the-art methods.

2. Background

Deformable image registration refers to the process of warping one moving image M to align with the fixed image F with a non-linear transformations [1]. This is an ill-posed issue in that task-unconcerned regions exist which can limit the alignment of regions of interest (ROIs) within a pair of images. Therefore, a region-aware spatial transformation is essential in such problems. Here, let M and F denote the moving and the fixed images respectively, and both are defined over an n -dimensional space domain Ω . The current deformable image registration approaches, the affine and scaling transformations have been factored such that the only source of misalignment between the images is non-linear. We follow this assumption throughout this paper, all the moving images M and fixed images F are linearly aligned via a preprocessing step [17]. For the rest of this paper, we focus on the case $n = 3$ but our method and implementation are dimension independent. We model a function $\mathcal{F}_\theta(F, M) = \Phi$ using a CNN, where Φ represents the deformation flow displacements (DFFs) and θ are neural network parameters. For each voxel $\mathbf{x} \in \Omega$, $\Phi(\mathbf{x})$ is a location such that $F(\mathbf{x})$ and $M(\mathbf{x})$ define similar anatomical locations and the typical deformable image registration

is formulated as:

$$\hat{\Phi} = \arg \min_{\Phi} \mathcal{T}_{sim}(F, M \circ \Phi) + \lambda \mathcal{R}_{smooth}(\Phi), \quad (1)$$

where $\hat{\Phi}$ denotes the optimal DFFs Φ , $\mathcal{T}_{sim}(\cdot, \cdot)$ denotes the image similarity loss function, $\mathcal{R}_{smooth}(\cdot)$ represents the smoothness regularization function, and λ is a regularization hyperparameter. The composition operation \circ denotes spatially transforming the moving image according to Φ . Traditional framework evaluates the global similarity of by optimizing problem in Eq. (1) for any new pair of images F and M , which is a slow process. The recent learning-based deformable image registration methods use a set of image pairs to train a convolutional neural network (CNN) to achieve fast registration [4, 8]. This method defines a deformation flow fields function $\mathcal{F}_\theta(F, M) \rightarrow \Phi$, which feeds the moving image M and a global flow transformation Φ to spatial transformer network (STN) to obtain the warped image $W = M \circ \Phi$ by a global similarity metric. In this work, we not only train this network to produce global spatial transformations, but also to learn region-aware spatial transformations that are capable of maximizing the similarity of ROIs within images.

3. Related Work

3.1. Learning-based Deformable Registration Methods

Learning-based deformable registration methods take advantage of GPU’s powerful computing ability to inference the deformation flow displacements (DFFs) to achieve rapid registration [14, 31]. Recently, there are many strategies [4, 5, 16, 21, 24, 31, 41, 41] regarding deformable image registration. Mok et al. [31] proposed a fast symmetric diffeomorphic image registration network (SYMNet), which maximizes the similarity of a pair of images to improve registration accuracy. Huang et al. [21] proposed a coarse-to-fine network architecture consisting of affine and deformable transformations (ACNet) to achieve accurate registration with global similarity constraint. While these methods learn the all anatomies structure registration to maximize the global similarity of a pair of images, which easily leads to mis-alignment on regions of interest (ROIs) within images. Moreover, these methods never pay attention to region similarity constraint of a pair of images, which cannot maintain the similarity of ROIs within images. Furthermore, label-constraint (LC) registration methods [5, 13, 15, 18–20, 27, 30, 42] maximize the global similarity of a pair of images with segmentation labels via a CNN. Balakrishnan et al. [5] proposed a supervised method to learn the similarity of a pair of images by leveraging a auxiliary information such as segmentation maps during training, which effectively improves registration accuracy.

Li et al. [27] proposed a deformable medical image registration with perception-correspondence and reverse teaching to learn global similarity metric by using segmentation labels during training, which improves registration accuracy. However, these methods only use appearance information without texture constraints, which leads to distortion on the ROIs. Moreover, these methods still use the global similarity to evaluate registration accuracy, which cannot maximize region similarity of a pair of images.

3.2. Similarity Evaluation in Deformable Image Registration

Learning similarity evaluation is a fundamental problem in deformable image registration [31]. Many similarity metrics [1, 5] have been developed in the context of deep learning (DL) for maximizing the similarity of a pair of images. Unsupervised DL-based deformable registration methods [4, 16, 21, 31, 41, 41] learn image similarity to align a pair of images using a global similarity metric such as normalized cross-correlation (NCC), mean squared error (MSE), sum of squares distance (SSD) and mutual information (MI). Label-constrained (LC) registration methods [5, 27, 30, 42] learn the mixed similarity of image by using segmentation labels via similarity metric. Although LC registration methods take auxiliary information to guide the network to perceive ROIs within images, these methods still maximize the global similarity of a pair of images, which cannot guarantee region similarity of a pair of images. In this work, we firstly pay attention to region similarity of a pair of images, a novel region consistency constraint is developed to maximize the similarity of ROIs within a pairs of images.

4. Dual-Flow Transformation Network

In this paper, we propose a novel dual-flow transformation network with region consistency constraint to achieve end-to-end registration, which is composed of two modules including region-aware flow transformation module and global flow transformation module. Let M and F denote the moving and the fixed images respectively, and both are defined over an n -dimensional space domain Ω . We take a function $\mathcal{F}_\theta(F, M) = \Phi$ to learn the displacement flow fields (DFFs) via a convolutional neural network (CNN), where Φ represents the DFFs and θ are neural network parameters. For each voxel $\mathbf{x} \in \Omega$, $\Phi(\mathbf{x})$ is a location such that $F(\mathbf{x})$ and $M(\mathbf{x})$ define similar anatomical locations.

4.1. Region-Aware Flow Transformation

As shown in Fig.1, the moving image M and the fixed image F are put into the segmentation CNN (Seg-CNN) to obtain the moving segmentation s'_M and fixed segmentation s'_F in N semantic channels without texture preservation.

Then the s'_M and s'_F multiply with the original images of M and F to obtain the regions of interest (ROIs) of moving image R_M and the ROIs of fixed image R_F , respectively. Hence, ROIs with texture-preserved are perceived as the inputs of registration CNN, which obviates interference with each other between ROIs and task-unconcerned regions during training. In this work, the cross-entropy loss function is used to calculate on segmentation loss with the fixed labels s_F and moving labels s_M , which is written as:

$$\mathcal{L}_{seg}(s, s') = -\frac{1}{NL} \sum_{n=0}^N \sum_{l=0}^L s_{l,n} \log s'_{l,n}, \quad (2)$$

where N is the number of the semantic channels from the Seg-CNN, the L is the number of the voxels in each semantic channel, the s is the segmentation label and the s' is the segmentation.

The ROIs within a pair of images are obtained using a Seg-CNN, and then the registration CNN (Reg-CNN) is employed to gain a region-aware flow filed for achieving alignment of ROIs between a pair of images. As shown in Fig.1, ROIs (R_M, R_F) of the moving and fixed images with texture-preserved are put into the Reg-CNN to obtain region-aware flow fields Φ_{Region} . The region-aware flow fields are used to deform R_M and M using spatial transformer network (STN) [22] to obtain the warped ROIs within moving image R_{W_M} and the warped moving image W_{R_M} , respectively. Similar to the existing DL-based methods [31], the local normalized cross-correlation (LNCC) is used as similarity metric (\mathcal{L}_{sim}) to evaluate the similarity of a pair of images. Let R_F and R_M denote a pair of input images, $\bar{R}_F(\mathbf{x})$ and $\bar{R}_M(\mathbf{x})$ denote the local mean of $R_F(\mathbf{x})$ and $R_M(\mathbf{x})$ at position \mathbf{x} respectively. Hence, region-aware LNCC (RLNCC) is written as:

$$RLNCC(R_F, R_M) = \sum_{\mathbf{x} \in \Omega} \frac{\sum_{\mathbf{x}_i} (R_F(\mathbf{x}_i) - \bar{R}_F(\mathbf{x}))(R_M(\mathbf{x}_i) - \bar{R}_M(\mathbf{x}))}{\sqrt{\sum_{\mathbf{x}_i} (R_F(\mathbf{x}_i) - \bar{R}_F(\mathbf{x}))^2 (R_M(\mathbf{x}_i) - \bar{R}_M(\mathbf{x}))^2}}, \quad (3)$$

where \mathbf{x}_i denotes the position local region centered at \mathbf{x} . Minimizing \mathcal{L}_{sim} will facilitate R_M to approximate R_F , however, this may obtain a non-smooth Φ . To mitigate this problem, a diffusion regularizer [5] on the spatial gradients of deformation flow fields is used to obtain a smooth Φ :

$$\mathcal{L}_{smooth}(\Phi_{Region}) = \sum_{\mathbf{x} \in \Omega} \|\nabla \Phi(\mathbf{x})\|^2, \quad (4)$$

where the spatial gradients are approximated using differences between neighboring voxels. Hence, we combine \mathcal{L}_{sim} with \mathcal{L}_{smooth} to obtain the region-aware loss function of ROIs for a pair of images:

$$\mathcal{L}_{Region}(R_F, R_M, \Phi_{Region}) = \mathcal{L}_{sim}(R_F, R_M) + \alpha \mathcal{L}_{smooth}(\Phi_{Region}), \quad (5)$$

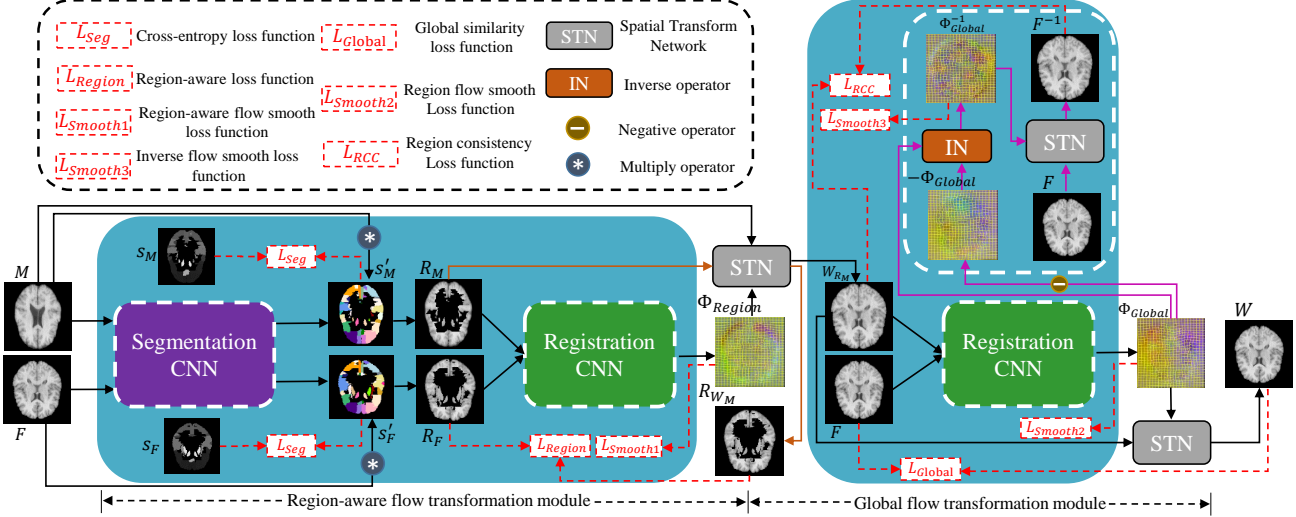


Figure 1. Overall architecture of our Dual-FlowNet. We utilize the segmentation CNN to gain the segmentation of input images both M and F , and then the segmentation results multiply with the original images to obtain R_M and R_F , respectively. The registration CNNs are used to learn region flow fields Φ_{Region} and global flow fields Φ_{Global} , respectively. Meanwhile, region consistency constraint \mathcal{L}_{RCC} is proposed to the consistency of region flow transformation and global flow transformation.

where α is a weight parameter to balance two loss functions.

4.2. Global Flow Transformation

Although the warped image of ROIs between the moving and fixed images is obtained, there still is a non-negligible issue. Only using few-shot datasets learn a Seg-CNN, which leads to imprecisely segmentations, thus losing potential ROIs within images. To further improve the registration accuracy of a pair of images, global flow transformation is designed to achieve a fine registration. Meanwhile, a region consistency constraint is developed to maximize the similarity ROIs between W_{R_M} and F . As shown in Fig.1, the region-aware warped image W_{R_M} and fixed image F are put into the registration CNN (Reg-CNN) to obtain a global flow field Φ_{Global} . Then Φ_{Global} is used to deform W_{R_M} using a STN [22], thus the global warped image W is predicted. Similar to region-aware flow transformation, LNCC is employed to evaluate the similarity of alignment between W_{R_M} and F . Hence, global LNCC (GLNCC) is written as:

$$GLNCC(F, W_{R_M}) = \sum_{\mathbf{x} \in \Omega} \frac{\sum_{\mathbf{x}_i} (F(\mathbf{x}_i) - \bar{F}(\mathbf{x}))(W_{R_M}(\mathbf{x}_i) - \bar{W}_{R_M}(\mathbf{x}))}{\sqrt{\sum_{\mathbf{x}_i} (F(\mathbf{x}_i) - \bar{F}(\mathbf{x}))^2 (W_{R_M}(\mathbf{x}_i) - \bar{W}_{R_M}(\mathbf{x}))^2}}, \quad (6)$$

where \mathbf{x}_i denotes the position local region centered at \mathbf{x} . Minimizing \mathcal{L}_{sim} will facilitate W_{R_M} to approximate F . Meanwhile, a diffusion regularizer function [5] on the spatial gradients of global flow fields is used to obtain a smooth

Φ_{Global} :

$$\mathcal{L}_{smooth}(\Phi_{Global}) = \sum_{\mathbf{x} \in \Omega} \|\nabla \Phi(\mathbf{x})\|^2, \quad (7)$$

where $\nabla \Phi(\mathbf{x}) = (\frac{\partial \Phi(\mathbf{x})}{\partial x}, \frac{\partial \Phi(\mathbf{x})}{\partial y}, \frac{\partial \Phi(\mathbf{x})}{\partial z})$ represents the calculation of gradients. By limiting the gradient of the deformation flow field, a smooth global flow field is obtained, thus extreme pixel displacement can be avoided. Therefore, we combine \mathcal{L}_{sim} with \mathcal{L}_{smooth} to obtain the global loss function of a pair of images:

$$\mathcal{L}_{Global}(F, W_{R_M}, \Phi_{Global}) = \mathcal{L}_{sim}(F, W_{R_M}) + \beta \mathcal{L}_{smooth}(\Phi_{Global}), \quad (8)$$

where β is a weight parameter to balance two loss functions.

4.3. Region Consistency Constraint

Existing learning-based approaches [5, 21, 31, 38, 39, 41] often maximize the global similarity of a pair of images by evaluating a similarity loss function, such as a normalized cross-correlation. Although the similarity of a pair of images can be effectively evaluated, the global similarity may greatly limit the registration accuracy due to the interference of task-unconcerned regions. Furthermore, these global similarity metrics are not sufficient to maximize the similarity of ROIs within images. To address this issue, we propose a novel region consistency constraint to guide fine registration of ROIs within a pair of images.

Intuitively, the registration process should be symmetrical, which refers to the bi-directional transformations between the moving image and the fixed image [3]. As shown

in Fig. 1, for flow Φ_{Global} , we firstly obtain its negative flow $-\Phi_{Global}$ via an negative operation [46]. We then feed both Φ_{Global} and $-\Phi_{Global}$ to the grid sampling module [22] to obtain the estimated inverse flow Φ_{Global}^{-1} . The inverse flow field Φ_{Global}^{-1} is defined as follows:

$$\Phi_{Global}^{-1} = \mathcal{I}(\Phi_{Global}, -\Phi_{Global}), \quad (9)$$

where $\mathcal{I}(\cdot, \cdot)$ denotes an inverse network. To guide ROIs within moving image to align with the ROIs within fixed image, we combine the fixed image F with the estimated inverse flow Φ_{Global}^{-1} to feed STN to predict inverse transformed image F^{-1} , which is written as:

$$F^{-1} = \mathcal{S}(F, \Phi_{Global}^{-1}), \quad (10)$$

where $\mathcal{S}(\cdot, \cdot)$ represents a STN. We use LNCC to evaluate the similarity of registration between F^{-1} and W_{R_M} . Meanwhile, the diffusion regularizer function [5] is used to obtain a smooth Φ_{Global}^{-1} . Hence, we combine $\mathcal{L}_{sim}(M^{-1}, F_{R_M})$ with $\mathcal{L}_{smooth}(\Phi_{Global}^{-1})$ to obtain the region consistency loss function:

$$\begin{aligned} \mathcal{L}_{RCC}(F^{-1}, W_{R_M}, \Phi_{Global}^{-1}) &= \mathcal{L}_{sim}(F^{-1}, W_{R_M}) \\ &+ \gamma \mathcal{L}_{smooth}(\Phi_{Global}^{-1}), \end{aligned} \quad (11)$$

where γ is a weight parameter to balance two loss functions. Minimizing \mathcal{L}_{RCC} will encourage W_{R_M} to approximate F^{-1} , which guides R_M to approximate R_F . Furthermore, the R_M approximates to R_F , which encourages the M to approximate F . Therefore, the region consistency of a pair of images is effectively preserved, and the complete loss function of our Dual-FlowNet can be written as:

$$\mathcal{L}(F, M) = \mathcal{L}_{Region} + \mathcal{L}_{Global} + \eta \mathcal{L}_{RCC} \quad (12)$$

where η is a weight parameter to balance the contributions of the region consistency constraint loss.

4.4. Network Details

As shown in Fig. 2 (a), our Seg-CNN segments the mask of ROI on the fixed and moving images. It follows U-Net structure [36], which consists of a four-level hierarchical encoder-decoder with skip connections. For each level in the encoder, we use two successive convolution layers followed by a group normalization (GN) [43] and a rectified linear units (ReLU), which contains one $3 \times 3 \times 3$ convolution layer with a stride of 1, and is followed by one $3 \times 3 \times 3$ convolution layer with a stride of 2 to down-sample the feature maps in half until the lowest level is reached. For each level in the decoder, we concatenate the feature maps from the encoder through skip connection, and one $3 \times 3 \times 3$ deconvolution with a stride of 2 is used to up-sample. The concatenation in the same resolution stage adds the detailed

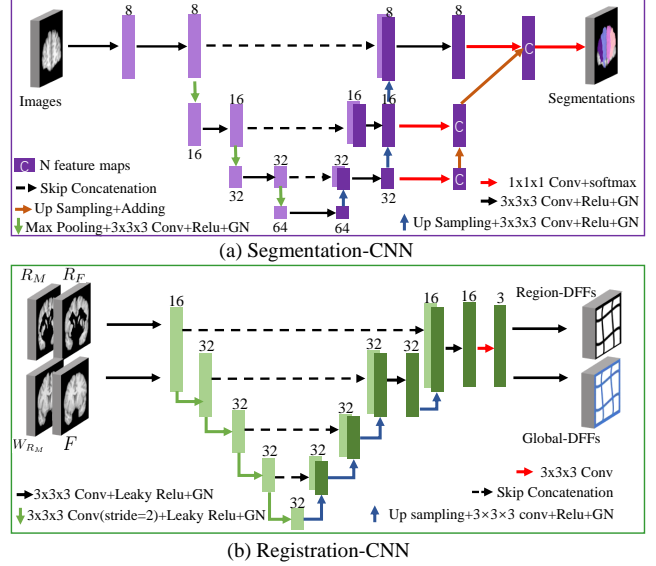


Figure 2. Detailed network structures of Seg-CNN and Reg-CNN.

information to the decoder. Each resolution stage in decoder outputs the segmentation via one $1 \times 1 \times 1$ convolutions for deep supervision. As shown in Fig. 2 (b), the ROIs within a pair of images are put into our Reg-CNN to obtain region deformable flow fields (DFFs). Similarly, the warped image and the fixed images are put into a Reg-CNN to obtain global DFFs. Reg-CNN follows the 3D U-Net structures [7] with five-level hierarchical encoder-decoder. In the encoder, each resolution stage has one $3 \times 3 \times 3$ convolution layer, and maxpooling is used to down-sample the feature maps between each stage. In the decoder, the first two stages have one $3 \times 3 \times 3$ convolution and the last two stage has two $3 \times 3 \times 3$ convolution for finer estimation in details. Each convolution is followed by a GN [43] and a ReLU. Finally, one $1 \times 1 \times 1$ convolution is used to estimate a DFF with three channels for the deformation of each voxel in x, y, z direction.

5. Experimental results

In this section, we evaluate our Dual-FlowNet on four public of 3D MRI image datasets. To further verify the effectiveness of our Dual-FlowNet, ablation study is provided on LPBA40 dataset.

5.1. Experimental configuration

5.1.1 Baseline methods

To demonstrate the superiority of our Dual-FlowNet, we compare with five state-of-the-art (SOTA) learning-based registration methods including RCN [47], LC-VoxelMorph [5], SYMNet [31], ACNet [10] and PC-Reg-RT [27]. The RCN [47] uses NCC loss function together with the smooth

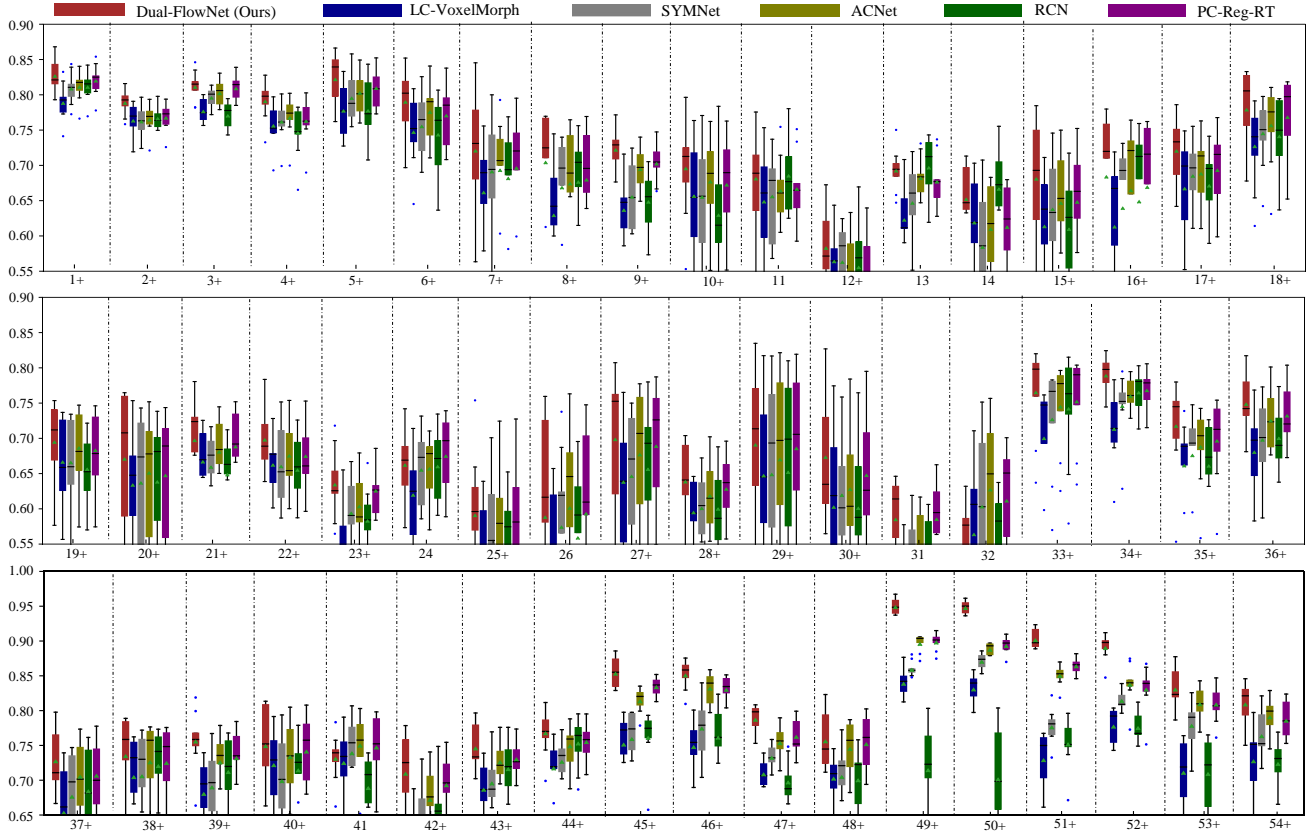


Figure 3. Boxplots of DSC values of 54 ROIs for the 10 testing subjects from the LPBA40 dataset. Our Dual-FlowNet compares with five SOTA registration methods including LC-VoxelMorph [5], SYMNet [31], ACNet [21], RCN [47] and PC-Reg-RT [27]. "+" marks statistically significant improvements given by our Dual-FlowNet over the other five SOTA methods.

	Dataset	LC-VoxelMorph	SYMNet	ACNet	RCN	PC-Reg-RT	Dual-FlowNet
DSC (%)	LPBA40	68.8 ± 1.5	69.3 ± 1.4	70.1 ± 1.6	71.8 ± 2.3	72.1 ± 1.5	75.3 ± 1.1
	IBSR18	56.8 ± 2.0	57.2 ± 1.3	57.4 ± 1.7	57.8 ± 2.7	58.5 ± 1.7	61.7 ± 1.5
	CUMC12	53.5 ± 2.7	54.2 ± 2.6	54.4 ± 2.1	54.4 ± 2.9	55.1 ± 2.5	58.1 ± 2.4
	MGH10	61.4 ± 2.3	61.5 ± 2.0	61.7 ± 2.0	61.7 ± 2.1	62.2 ± 1.9	65.9 ± 1.4
ASD (mm)	LPBA40	0.54 ± 0.09	0.52 ± 0.04	0.50 ± 0.03	0.47 ± 0.03	0.46 ± 0.03	0.31 ± 0.02
	IBSR18	0.72 ± 0.08	0.69 ± 0.04	0.68 ± 0.06	0.68 ± 0.05	0.67 ± 0.04	0.59 ± 0.03
	CUMC12	0.75 ± 0.09	0.73 ± 0.08	0.71 ± 0.05	0.70 ± 0.04	0.69 ± 0.02	0.62 ± 0.02
	MGH10	0.61 ± 0.07	0.59 ± 0.04	0.58 ± 0.05	0.58 ± 0.04	0.57 ± 0.03	0.49 ± 0.02

Table 1. Comparison of DSC and ASD for five SOTA methods including LC-VoxelMorph [5], SYMNet [31], ACNet [21], RCN [47] and PC-Reg-RT [27] in LPBA40, IBSR18, CUMC12 and MGH10. The best results are identified in bold.

loss. The LC-VoxelMorph [5] uses Dice loss together with the smooth loss by leveraging segmentation labels, and the NCC loss is used to evaluate the similarity of a pair of images. The SYMNet [31] employs orientation consistency loss together with the smooth loss and magnitude loss to obtain smooth deformation voter displacement, the NCC loss is used to evaluate the similarity of a pair of images. The ACNet [10] uses NCC loss together with dual consistency

constraint to evaluate the similarity of a pair of images. The PC-Reg-RT [27] employs NCC loss function together with the smooth loss.

5.1.2 Datasets

To evaluate performance of the proposed method in deformable image registration, we use four public datasets on

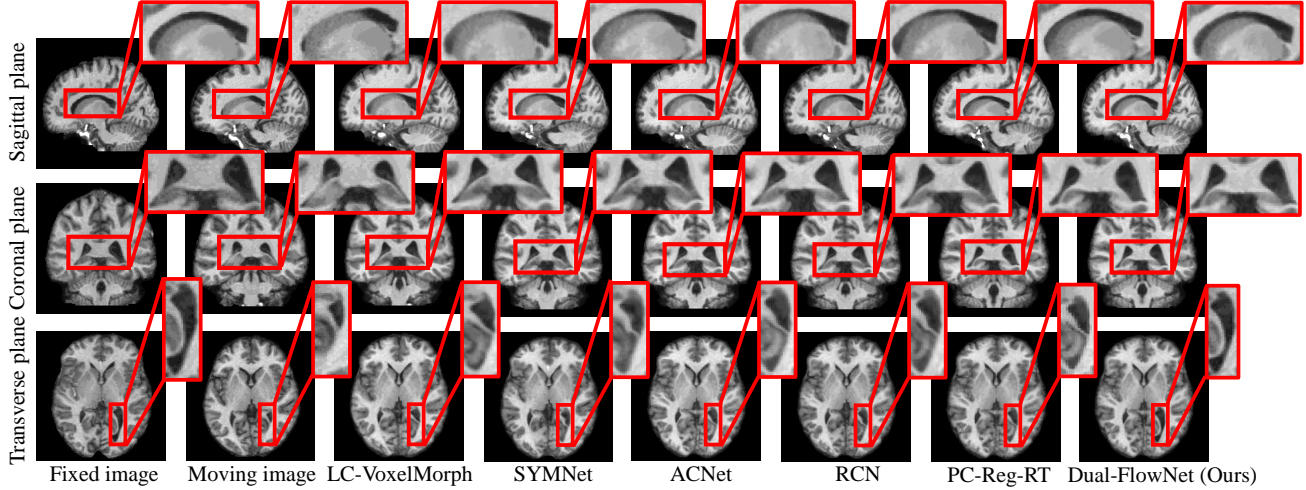


Figure 4. Typical registration results in sagittal plane, coronal plane and transverse plane from MGH10 dataset. Our Dual-FlowNet compares with five SOTA registration methods including LC-VoxelMorph [5], SYMNet [31], ACNet [21], RCN [47] and PC-Reg-RT [27]. The red rectangles in the figure elaborate the registration comparison of ROIs. Only image slices are presented but note that the registration is actually performed in 3D.

two types of 3D MRI images: LPBA40 (LONI Probabilistic Brain Atlas)¹, this dataset contains 40 scans, each of which comes with segmentation ground truth of 56 anatomical structures. IBSR18², this dataset contains 18 scans, each of which comes with segmentation ground truth of 128 anatomical structures. CUMC12 and MGH10 datasets³, which contains 12 and 10 scans, respectively. Brain MRI images are resampled to the same size ($160 \times 192 \times 160$) to fit the input size of network. LPBA40 contains 40 subjects, 30 subjects are selected for training and the remaining 10 subjects are used for validation. Besides, IBSR18, CUMC12 and MGH10 are used to evaluate the generalization performance of the proposed method.

5.1.3 Implementation details

All methods are based on an initialization via affine transformation [23]. Our Dual-FlowNet and other comparative DL-based methods are all implemented by Pytorch [35] on an Intel i7-7700 CPU and an NVIDIA GTX1080Ti GPU with 12GB memory. We set $\alpha = \beta = \gamma = 1$ for our Dual-FlowNet to achieve accurate registration performance, meanwhile, the smooth DFFs follow the setting of LC-VoxelMorph [5] in our experiments. The η is 0.5, so that the similarity of ROIs within images will be maximized by using our region consistency constraint. All DL-based meth-

¹The LPBA40 dataset is available at: <https://resource.loni.usc.edu/resources/atlas-downloads/>.

²The IBSR18 dataset is available at: <https://www.nitrc.org/projects/ibsr/>.

³CUMC12 and MGH10 datasets are available at: <https://continuousregistration.grand-challenge.org/rules/>.

ods are optimized by Adam whose learning rate is 1×10^{-4} . The training batch size is 1 to save the memory. Our implementation includes a default of 20,000 iterations. To improve the generalization ability, the random mirror in x , y and z -axis, and rotation in $[-25^\circ, 25^\circ]$ are conducted for data augmentation.

5.1.4 Evaluation metrics

The registration performance is quantified by using Dice score (DSC) [11] and average symmetric surface distance (ASD) based on the segmentation of some anatomical structure, between the warped moving image and the fixed image, as done in [5, 27]. The DSC and ASD of two regions W, F are respectively formulated as:

$$\text{Dice}(W, F) = 2 \cdot \frac{|W \cap F|}{|W| + |F|}. \quad (13)$$

The higher of DSC means the better accuracy of registration. Perfectly overlapped regions come with a DSC of 1.

$$\text{ASD}(W, F) = \frac{1}{|S(W)| + |S(F)|} \left(\sum_{\mathbf{s}_W \in S(W)} d(s_W, S(F)) + \sum_{\mathbf{s}_F \in S(F)} d(s_F, S(W)) \right), \quad (14)$$

where $S(\cdot)$ denotes the set of surface voxel of W and the $d(\cdot, \cdot)$ represents the shortest distance of an arbitrary voxel \mathbf{x} to $W(\mathbf{x})$. The lower of ASD means the better accuracy of registration.

	GFN	RFN	GRFN	DFN
D	68.6 ± 1.9	60.3 ± 2.8	70.7 ± 1.5	75.3 ± 1.1
A	0.64 ± 0.09	1.33 ± 0.28	0.53 ± 0.07	0.31 ± 0.02

Table 2. Ablation study analyses the effectiveness of Dual-FlowNet. The GFN, RFN, GRFN and DFN denote G-FlowNet, R-FlowNet, GR-FlowNet and Dual-FlowNet, respectively. The D and A represent DSC (%) and ASD (mm), respectively. The best results are identified in bold.

5.2. 3D Brain MRI registration experiments

5.2.1 Evaluation on LPBA40

In order to verify the superiority of our Dual-FlowNet, we test 10 subjects in LPBA40 dataset. The DSC of 54 ROIs [25] in test subjects is respectively shown in Fig. 3, and the average DSC is provided in Table 1. It is shown that our Dual-FlowNet achieves the best performance for 46 out of the 54 ROIs. The performance for the remaining 8 ROIs is comparable with other SOTA methods. Our region-aware spatial transformation firstly perceives ROIs with texture information to eliminate mis-alignment and weaken distortion. Furthermore, a global spatial transformation is used to further dig out potential ROIs, thus achieving accurate registration results.

5.2.2 Evaluation on IBSR18, CUMC12, MGH10

To demonstrate the generalization performance of our Dual-FlowNet, the trained model on LPBA40 dataset is utilized to test other three 3D MRI datasets including IBSR18, CUMC12, and MGH10. The average DSC and ASD are provided in Table 1, our Dual-FlowNet achieves the best registration results. Competing other five methods, our Dual-FlowNet pays attention to maintain the similarity of ROIs within images. Moreover, RCC is used to guide network to adequately explore the potential ROIs, thus achieving fine registration. As is shown in Fig.4, a typical result from MGH10 is shown that our Dual-FlowNet has region-aware ability and guarantees clear texture feature, thus our Dual-FlowNet achieves the best registration results.

5.3. Ablation study

To further verify the effectiveness of our Dual-FlowNet, ablation study is provided on LPBA40 dataset.

We design ablation experiments including four cases: 1) We only use global spatial transformation to align a pair of images without region spatial transformation and region consistency constraint (G-FlowNet); 2) We only use region spatial transformation to align a pair of images without region spatial transformation and region consistency constraint (R-FlowNet); 3) We use global spatial transformation and region spatial transformation to align a pair of images with-

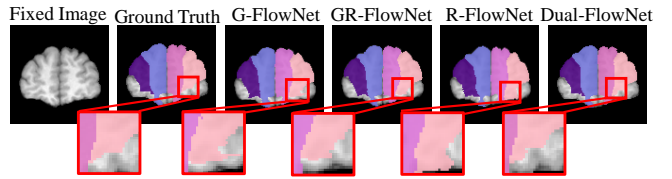


Figure 5. Registration example on LPBA40 dataset. The red rectangles in the figure emphasize the registration comparison of ROIs. Only image slices are presented but note that the registration is actually performed in 3D.

out region consistency constraint (GR-FlowNet); 4) We use global spatial transformation and region spatial transformation to align a pair of images with region consistency constraint (Dual-FlowNet). As is shown in Table 2, 30 subjects in LPBA40 dataset are selected to train network model, and 10 subjects are used to test DSC and ASD. It is clear that G-FlowNet obtains a baseline registration result due to not pay attention to region spatial transformation. In addition, R-FlowNet only uses ROIs within images to learn deformation flow fields with few-shot segmentation labels via a single CNN, which cannot obtain accurate ROIs, resulting in a poor registration result. After we combine global spatial transformation with region spatial transformation to align a pair of images, the registration results have a improvement. Furthermore, we use Dual-FlowNet to align a pair of images for testing DSC and ASD, our Dual-FlowNet has region-preserved ability to perceive ROIs and exploration competence for potential ROIs of image, which maximizes the similarity of ROIs within images, thus achieving excellent registration results. To further demonstrate the effectiveness of Dual-FlowNet, a typical example on LPBA40 dataset is provided in Fig. 5.

6. Conclusion

In this work, two ideas have been proposed: (i) a Dual-FlowNet is developed to eliminate mis-alignment and weaken distortion, and (ii) a region consistency constraint is proposed to guarantee the consistency of region spatial transformation and global spatial transformation, which maximizes the similarity of ROIs within a pair of images. Experiments on four public 3D MRI datasets are performed to show the superior performance of Dual-FlowNet, and experimental results demonstrate that Dual-FlowNet achieves better registration performances than other SOTA methods.

Limitations: Although our Dual-FlowNet outperforms SOTA methods in mono-modal registration, there still is a troublesome task in multi-modal registration. How to achieve great significance in multi-modal registration will be the focus of future work.

7. Broader Impact

Our Dual-FlowNet focuses on interest-region deformable registration, which can quantitatively analyze the changes of lesions and organs to enhance the accuracy and reliability of medical diagnosis, surgical plans, and radiotherapy plans.

References

[1] Ebrahim Al Safadi and Xubo Song. Learning-based image registration with meta-regularization. In *Proceedings of the IEEE/CVF Conference on Computer Vision and Pattern Recognition*, pages 10928–10937, 2021. [2](#), [3](#)

[2] Moab Arar, Yiftach Ginger, Dov Danon, Amit H Bermano, and Daniel Cohen-Or. Unsupervised multi-modal image registration via geometry preserving image-to-image translation. In *Proceedings of the IEEE/CVF conference on computer vision and pattern recognition*, pages 13410–13419, 2020. [1](#)

[3] Brian B Avants, Charles L Epstein, Murray Grossman, and James C Gee. Symmetric diffeomorphic image registration with cross-correlation: evaluating automated labeling of elderly and neurodegenerative brain. *Medical image analysis*, 12(1):26–41, 2008. [1](#), [4](#)

[4] Guha Balakrishnan, Amy Zhao, Mert R Sabuncu, John Guttag, and Adrian V Dalca. An unsupervised learning model for deformable medical image registration. In *Proceedings of the IEEE conference on computer vision and pattern recognition*, pages 9252–9260, 2018. [2](#), [3](#)

[5] Guha Balakrishnan, Amy Zhao, Mert R Sabuncu, John Guttag, and Adrian V Dalca. Voxelmorph: a learning framework for deformable medical image registration. *IEEE transactions on medical imaging*, 38(8):1788–1800, 2019. [1](#), [2](#), [3](#), [4](#), [5](#), [6](#), [7](#)

[6] Si-Yuan Cao, Hui-Liang Shen, Shu-Jie Chen, and Chun-guang Li. Boosting structure consistency for multispectral and multimodal image registration. *IEEE Transactions on Image Processing*, 29:5147–5162, 2020. [1](#)

[7] Özgün Çiçek, Ahmed Abdulkadir, Soeren S Lienkamp, Thomas Brox, and Olaf Ronneberger. 3d u-net: learning dense volumetric segmentation from sparse annotation. In *International conference on medical image computing and computer-assisted intervention*, pages 424–432. Springer, 2016. [5](#)

[8] Bob D de Vos, Floris F Berendsen, Max A Viergever, Marius Staring, and Ivana Isgum. End-to-end unsupervised deformable image registration with a convolutional neural network. In *Deep learning in medical image analysis and multimodal learning for clinical decision support*, pages 204–212. Springer, 2017. [2](#)

[9] Xin Deng and Pier Luigi Dragotti. Deep convolutional neural network for multi-modal image restoration and fusion. *IEEE transactions on pattern analysis and machine intelligence*, 2020. [1](#)

[10] Neel Dey, Mengwei Ren, Adrian V Dalca, and Guido Gerig. Generative adversarial registration for improved conditional deformable templates. In *Proceedings of the IEEE/CVF International Conference on Computer Vision*, pages 3929–3941, 2021. [1](#), [5](#), [6](#)

[11] Lee R Dice. Measures of the amount of ecologic association between species. *Ecology*, 26(3):297–302, 1945. [7](#)

[12] Yuhang Ding, Xin Yu, and Yi Yang. Modeling the probabilistic distribution of unlabeled data for one-shot medical image segmentation. In *Proceedings of the AAAI Conference on Artificial Intelligence*, volume 35, pages 1246–1254, 2021. [1](#)

[13] Koen A. J. Eppenhof and Josien P. W. Pluim. Pulmonary ct registration through supervised learning with convolutional neural networks. *IEEE Transactions on Medical Imaging*, 38(5):1097–1105, 2019. [1](#), [2](#)

[14] Jingfan Fan, Xiaohuan Cao, Qian Wang, Pew-Thian Yap, and Dinggang Shen. Adversarial learning for mono-or multi-modal registration. *Medical image analysis*, 58:101545, 2019. [2](#)

[15] Jingfan Fan, Xiaohuan Cao, Pew-Thian Yap, and Dinggang Shen. Birnet: Brain image registration using dual-supervised fully convolutional networks. *Medical image analysis*, 54:193–206, 2019. [2](#)

[16] Tobias Fechter and Dimos Baltas. One-shot learning for deformable medical image registration and periodic motion tracking. *IEEE transactions on medical imaging*, 39(7):2506–2517, 2020. [1](#), [2](#), [3](#)

[17] Vladimir Fonov, Alan C Evans, Kelly Botteron, C Robert Almlie, Robert C McKinstry, D Louis Collins, Brain Development Cooperative Group, et al. Unbiased average age-appropriate atlases for pediatric studies. *Neuroimage*, 54(1):313–327, 2011. [2](#)

[18] Shaikat M Galib, Hyoung K Lee, Christopher L Guy, Matthew J Ribblett, and Geoffrey D Hugo. A fast and scalable method for quality assurance of deformable image registration on lung ct scans using convolutional neural networks. *Medical physics*, 47(1):99–109, 2020. [1](#), [2](#)

[19] Yuting He, Tiantian Li, Guanyu Yang, Youyong Kong, Yang Chen, Huazhong Shu, Jean-Louis Coatrieu, Jean-Louis Dillenseger, and Shuo Li. Deep complementary joint model for complex scene registration and few-shot segmentation on medical images. In *Computer Vision–ECCV 2020: 16th European Conference, Glasgow, UK, August 23–28, 2020, Proceedings, Part XVIII 16*, pages 770–786. Springer, 2020. [1](#), [2](#)

[20] Yuting He, Guanyu Yang, Jian Yang, Yang Chen, Youyong Kong, Jiasong Wu, Lijun Tang, Xiaomei Zhu, Jean-Louis Dillenseger, Pengfei Shao, et al. Dense biased networks with deep priori anatomy and hard region adaptation: Semi-supervised learning for fine renal artery segmentation. *Medical image analysis*, 63:101722, 2020. [1](#), [2](#)

[21] Weijian Huang, Hao Yang, Xinfeng Liu, Cheng Li, Ian Zhang, Rongpin Wang, Hairong Zheng, and Shanshan Wang. A coarse-to-fine deformable transformation framework for unsupervised multi-contrast mr image registration with dual consistency constraint. *IEEE Transactions on Medical Imaging*, 2021. [1](#), [2](#), [3](#), [4](#), [6](#), [7](#)

[22] Max Jaderberg, Karen Simonyan, Andrew Zisserman, et al. Spatial transformer networks. *Advances in neural information processing systems*, 28:2017–2025, 2015. 3, 4, 5

[23] Mark Jenkinson and Stephen Smith. A global optimisation method for robust affine registration of brain images. *Medical image analysis*, 5(2):143–156, 2001. 7

[24] Boah Kim, Dong Hwan Kim, Seong Ho Park, Jieun Kim, June-Goo Lee, and Jong Chul Ye. Cyclemorph: Cycle consistent unsupervised deformable image registration. *Medical Image Analysis*, 71:102036, 2021. 2

[25] Arno Klein, Jesper Andersson, Babak A Ardekani, John Ashburner, Brian Avants, Ming-Chang Chiang, Gary E Christensen, D Louis Collins, James Gee, Pierre Hellier, et al. Evaluation of 14 nonlinear deformation algorithms applied to human brain mri registration. *Neuroimage*, 46(3):786–802, 2009. 8

[26] Jimmy Addison Lee, Peng Liu, Jun Cheng, and Huazhu Fu. A deep step pattern representation for multimodal retinal image registration. In *Proceedings of the IEEE/CVF International Conference on Computer Vision*, pages 5077–5086, 2019. 1

[27] Shuo Li, Yuting He, Tiantian Li, Rongjun Ge, Guanyu Yang, Jian Yang, Youyong Kong, Jian Zhu, and Huazhong Shu. Few-shot learning for deformable medical image registration with perception-correspondence decoupling and reverse teaching. *IEEE Journal of Biomedical and Health Informatics*, 2021. 1, 2, 3, 5, 6, 7

[28] Risheng Liu, Zi Li, Xin Fan, Chenying Zhao, Hao Huang, and Zhongxuan Luo. Learning deformable image registration from optimization: perspective, modules, bilevel training and beyond. *IEEE Transactions on Pattern Analysis and Machine Intelligence*, 2021. 1

[29] Jiayi Ma, Xingyu Jiang, Aoxiang Fan, Junjun Jiang, and Junchi Yan. Image matching from handcrafted to deep features: A survey. *International Journal of Computer Vision*, 129(1):23–79, 2021. 1

[30] Lucas Mansilla, Diego H Milone, and Enzo Ferrante. Learning deformable registration of medical images with anatomical constraints. *Neural Networks*, 124:269–279, 2020. 1, 2, 3

[31] Tony CW Mok and Albert Chung. Fast symmetric diffeomorphic image registration with convolutional neural networks. In *Proceedings of the IEEE/CVF conference on computer vision and pattern recognition*, pages 4644–4653, 2020. 1, 2, 3, 4, 5, 6, 7

[32] Xiaohan Nie, Shixing Chen, and Raffay Hamid. A robust and efficient framework for sports-field registration. In *Proceedings of the IEEE/CVF Winter Conference on Applications of Computer Vision*, pages 1936–1944, 2021. 1

[33] Marc Niethammer, Roland Kwitt, and Francois-Xavier Vialard. Metric learning for image registration. In *Proceedings of the IEEE/CVF Conference on Computer Vision and Pattern Recognition*, pages 8463–8472, 2019. 1

[34] Lingjiao Pan, Fei Shi, Dehui Xiang, Kai Yu, Luwen Duan, Jian Zheng, and Xinjian Chen. Octrexpert: a feature-based 3d registration method for retinal oct images. *IEEE Transactions on Image Processing*, 29:3885–3897, 2020. 1

[35] Adam Paszke, Sam Gross, Soumith Chintala, Gregory Chanan, Edward Yang, Zachary DeVito, Zeming Lin, Alban Desmaison, Luca Antiga, and Adam Lerer. Automatic differentiation in pytorch. In *NIPS-W*, 2017. 7

[36] Olaf Ronneberger, Philipp Fischer, and Thomas Brox. U-net: Convolutional networks for biomedical image segmentation. In *International Conference on Medical image computing and computer-assisted intervention*, pages 234–241. Springer, 2015. 5

[37] Daniel Rueckert, Luke I Sonoda, Carmel Hayes, Derek LG Hill, Martin O Leach, and David J Hawkes. Nonrigid registration using free-form deformations: application to breast mr images. *IEEE transactions on medical imaging*, 18(8):712–721, 1999. 1

[38] Roman Schaffert, Jian Wang, Peter Fischer, Anja Borsdorf, and Andreas Maier. Learning an attention model for robust 2-d/3-d registration using point-to-plane correspondences. *IEEE transactions on medical imaging*, 39(10):3159–3174, 2020. 1, 4

[39] Zhengyang Shen, Xu Han, Zhenlin Xu, and Marc Niethammer. Networks for joint affine and non-parametric image registration. In *Proceedings of the IEEE/CVF Conference on Computer Vision and Pattern Recognition*, pages 4224–4233, 2019. 1, 4

[40] Alena Uus, Tong Zhang, Laurence H Jackson, Thomas A Roberts, Mary A Rutherford, Joseph V Hajnal, and Maria Deprez. Deformable slice-to-volume registration for motion correction of fetal body and placenta mri. *IEEE transactions on medical imaging*, 39(9):2750–2759, 2020. 1

[41] Jian Wang and Miaoqiao Zhang. Deepflash: An efficient network for learning-based medical image registration. In *Proceedings of the IEEE/CVF conference on computer vision and pattern recognition*, pages 4444–4452, 2020. 1, 2, 3, 4

[42] Yiqian Wang, Junkang Zhang, Melina Cavichini, Dirk-Uwe G Bartsch, William R Freeman, Truong Q Nguyen, and Cheolhong An. Robust content-adaptive global registration for multimodal retinal images using weakly supervised deep-learning framework. *IEEE Transactions on Image Processing*, 30:3167–3178, 2021. 1, 2, 3

[43] Yuxin Wu and Kaiming He. Group normalization. In *Proceedings of the European conference on computer vision (ECCV)*, pages 3–19, 2018. 5

[44] Zhenguo Yang, Qing Li, Wenyin Liu, and Jianming Lv. Shared multi-view data representation for multi-domain event detection. *IEEE transactions on pattern analysis and machine intelligence*, 42(5):1243–1256, 2019. 1

[45] Zhuoqian Yang, Yang Yang, Kun Yang, and Zi-Quan Wei. Non-rigid image registration with dynamic gaussian component density and space curvature preservation. *IEEE Trans. Image Process.*, 28(5):2584–2598, 2018. 1

[46] Jun Zhang. Inverse-consistent deep networks for unsupervised deformable image registration. *arXiv preprint arXiv:1809.03443*, 2018. 5

[47] Shengyu Zhao, Yue Dong, Eric I Chang, Yan Xu, et al. Recursive cascaded networks for unsupervised medical image registration. In *Proceedings of the IEEE/CVF International*

Conference on Computer Vision, pages 10600–10610, 2019.

[5](#), [6](#), [7](#)

[48] Yuanjie Zheng, Xiaodan Sui, Yanyun Jiang, Tontong Che, Shaotong Zhang, Jie Yang, and Hongsheng Li. Symreg-gan: Symmetric image registration with generative adversarial networks. *IEEE Transactions on Pattern Analysis and Machine Intelligence*, 2021. 1